2021

Tunable Optical Filter Using Phase Change Materials for Smart IR Night Vision Applications

Remona Heenkenda
University of Dayton

Keigo Hirakawa
University of Dayton, khirakawa1@udayton.edu

Andrew Sarangan
University of Dayton, asarangan1@udayton.edu

Research Article | Vol. 29, No. 21 / 11 Oct 2021 / Optics Express 33795
Optics EXPRESS

Tunable optical filter using phase change materials for smart IR night vision applications

REMONA HEENKENDA,[1,*] KEIGO HIRAKAWA,[2] AND ANDREW SARANGAN[1]

[1]Department of Electro Optics, University of Dayton, 300 College Park, Dayton, OH 45469, USA
[2]Department of Electrical and Computer Engineering, University of Dayton, 300 College Park, Dayton, OH 45469, USA
[*]heenkendar1@udayton.edu

Abstract: In this paper we present a tunable filter using $Ge_2Sb_2Se_4Te_1$ (GSST) phase change material. The design principle of the filter is based on a metal-insulator-metal (MIM) cavity operating in the reflection mode. This is intended for night vision applications that utilize 850nm as the illumination source. The filter allows us to selectively reject the 850nm band in one state. This is illustrated through several daytime and nighttime imaging applications.

1. Introduction

Dynamically tunable optical filters have been highly sought after as an alternative to static filters. By altering its spectral transmittance or reflectance functions, dynamic filters can give an imaging system a *dual purpose functionality*. However, unlike static filters, tunable filters are much more difficult to fabricate. Materials whose refractive index can be electronically altered are rare, but it is even rarer for them to be compatible with standard deposition techniques, be capable of integration into standard multilayer optical stacks, and be usable in an end-application.

In this work, we demonstrate a novel tunable optical filter for smart IR night vision imaging systems. We consider the chalcogenide family of materials consisting of Ge, Sb, Te (commonly abbreviated as GST). The chalcogenide materials were developed in the 1960's as a nonvolatile electronic memory [1], and subsequently for optical data storage [2]. Known as phase change materials (PCM), they are capable of producing large and reversible changes in electrical resistivity and optical constants due to a physical re-arrangement of its crystal structure. In GST, this re-arrangement is induced by the application of a heat pulse, and it results in the material switching between amorphous and crystalline states. The most common composition of GST is $Ge_2Sb_2Te_5$. A large number of optical devices including tunable filters have already been realized using this material for different applications [3–8].

GSST is a newer phase change material that undergoes a similar phase transition, but at a higher transition temperature (approx 300°C instead of 150°C) [9]. It is synthesized by partially substituting selenium for tellurium, resulting in a composition of $Ge_2Sb_2Se_4Te_1$. This PCM has a lower optical loss and a larger index contrast between the two states compared to $Ge_2Sb_2Te_5$, making it better suited for optical applications than GST. Therefore, GSST was chosen as the active optical material in this work. Also, in a recent publication, large scale (up to 0.4mm), electrically reconfigurable GSST metasurfaces have been reported [10]. This proves the possibility of implementing a pixelated version of the proposed filter in smart IR systems that would enable real time reconfigurabilty.

The proposed filter design is a Metal-Insulator-Metal (MIM) cavity that can be easily fabricated as stratified layers without any complex patterning processes. Even though MIM has been used previously in tunable optical filter designs with PCMs [8,11,12], none of them presented a systematic approach for designing these structures. In this paper, we introduce a well formed

#440299 https://doi.org/10.1364/OE.440299
Journal © 2021 Received 12 Aug 2021; revised 17 Sep 2021; accepted 19 Sep 2021; published 30 Sep 2021

Optics EXPRESS

theory for designing MIM as well as for incorporating PCMs which can be easily adapted to other wavelengths, configurations and applications.

2. Motivation

For our application, we consider silicon-based cameras which typically cover both visible and near-infrared (NIR) wavelengths up to 1μm. Color cameras designed for human consumption commonly use a short-pass filter to attenuate the NIR photons so that the spectral transmittance of color filters in the 400-720nm range can be better matched to the color perception of human vision. This short-pass filtering is particularly important during the daytime, as solar radiation has significant strength in the NIR wavelengths.

The goal of this work is to enable night vision while maintaining proper daytime color imaging. Night vision systems typically utilize NIR LEDs or lasers (such as 850nm and 950nm) as the illumination source. The ability to operate in visible and NIR wavelengths has many interesting applications, such as driver-assistive automotive technology, surveillance and other human-in-the-loop imaging systems. For instance, NIR illumination can be used even at oncoming traffic as well as with rear-facing headlights. However, conventional color cameras equipped with a short-pass filter will not be compatible with this dual-band operation. Instead, current-generation dual-band systems use multiple sensors (one for color, one for NIR). Another approach is to use a dual-bandpass filter (such as the one shown in Fig. 2(b)) that allows a small portion of the NIR illumination wavelength to pass through. This is an interim solution because even a small NIR passband degrades the color representation during daytime usage. One potential solution to this problem is to have a mechanical device that adds a short-pass filter in front of the silicon detector during daytime operations. However, devices such as mechanical sliders often fail in long-term usage due to wear-and-tear, with unfavorable cost and size implications.

A more desirable solution is to employ a dynamically tunable optical filter that can pass or attenuate near-IR wavelengths without any moving parts. Such switchable filters would give dual purpose functionality (color imaging and NIR imaging) to a silicon-based detector. In this paper, we demonstrate the design, fabrication and imaging performance of a 850nm switchable optical notch filter using a phase change material (GSST). Specifically, this filter was designed to pass light near 850nm in its crystalline state but attenuate it in its amorphous state.

3. Design principle

The design of our tunable GSST filter is based on the metal-insulator-metal (MIM) resonant optical cavity. MIM cavities can be systematically designed using the effective reflectance index method [13]. In brief, this method mathematically collapses the entire layer structure into a single effective index for the purposes of calculating the reflection. To achieve resonance at a desired wavelength λ, the entire stack has to collapse to an absentee layer—i.e., it has to become a multiple of half-wave phase, or a round trip phase that is a multiple of 2π.

The effective reflectance index is a lumped equivalent index parameter for a multilayer structure that can be directly used in the Fresnel equation for reflection:

$$r = \frac{n_r - n_a}{n_r + n_a} \tag{1}$$

where n_r is the effective reflectance index and n_a is the refractive index of the incident medium. Resonance condition at a given wavelength is achieved when n_r becomes equal to n_a, and reflection falls to zero. All of the layer details are essentially contained in the effective reflectance index n_r. The expressions for n_r can be derived from first principles [13]. These are:

$$n_{r_1} = n_{f_1} \frac{(n_s + n_{f_1}) + (n_s - n_{f_1})e^{-j\theta_1}}{(n_s + n_{f_1}) - (n_s - n_{f_1})e^{-j\theta_1}}, \tag{2}$$

Optics EXPRESS

$$n_{r_2} = n_{f2}\frac{(n_{r_1} + n_{f_2}) + (n_{r_1} - n_{f_2})e^{-j\theta_2}}{(n_{r_1} + n_{f_2}) - (n_{r_1} - n_{f_2})e^{-j\theta_2}}, \tag{3}$$

$$n_{r_3} = n_{f_3}\frac{(n_{r_2} + n_{f_3}) + (n_{r_2} - n_{f_3})e^{-j\theta_3}}{(n_{r_2} + n_{f_3}) - (n_{r_2} - n_{f_3})e^{-j\theta_3}}, \tag{4}$$

where the phase thicknesses of each layer under normal incidence are $\theta_1 = 2k_0 n_{f_1} a_1$, $\theta_2 = 2k_0 n_{f_2} a_2$ and $\theta_3 = 2k_0 n_{f_3} a_3$. This has to be computed recursively starting from n_{r_3} and ending in n_{r_1}. The resulting n_{r_1} is the lumped equivalent index parameter that represents all layers including the substrate. To satisfy the resonance condition, final effective reflectance index (n_{r_3}) should be equal to the refractive index of the incident medium (n_a). The thicknesses of the MIM cavity for a given set of materials at a given wavelength can be calculated using this condition. Thus, for a given metal thickness (M1) and dielectric thickness (H), the second metal thickness (M2) can be calculated by solving the complex contours plotted using Eq. (3) and 4 of the effective reflectance index. Further details of this method can be found in [13] and [14].

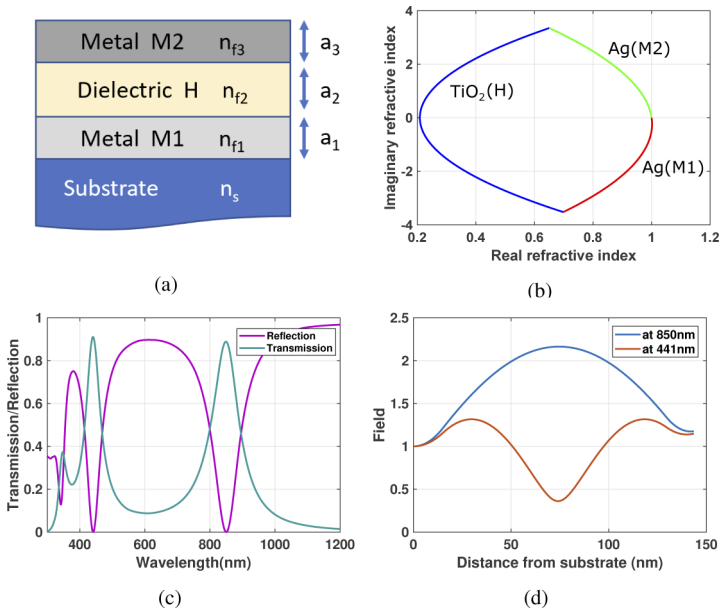

Fig. 1. (a) MIM single-cavity structure with thicknesses a_1, a_2, and a_3 with refractive indices n_{f1}, n_{f2}, and n_{f3}, (b) Solved contour plot for the MIM cavity using effective reflectance index method, (c) Reflection/transmission plot using TMM for the structures in (a) and (d) Field intensity plot for the cavity.

To simplify the discussion, we will assume the substrate is AR (anti-reflection) coated. Figure 1 is an example of a solved contour plot of MIM cavity designed at 850nm using Ag(M1)/TiO_2(H)/Ag(M2). The solved thickness of the TiO_2 is 114 nm and the silver layer thicknesses are 15 nm and 14 nm. The solution forms a complete contour making the round trip phase to be 2π (Fig. 1(b)). The reflection and transmission spectra for these structures can be calculated using TMM (Transfer Matrix Method), which is shown in Fig. 1(c). We can see that in addition to the fundamental resonance at 850nm, the cavity also exhibits a 2^{nd} order resonance at 440nm. Although one might expect this 2^{nd} order resonance to occur at half the fundamental wavelength (which would be 425nm), due to material dispersion (which is especially significant in metals) it may be slightly shifted and/or it may be an imperfect resonance (i.e. reflection may not fall to an exact zero). Additionally, we can also see from Fig. 1(d) that the field intensity at

Optics EXPRESS

850nm has a maximum at the center of the cavity (fundamental resonance), and the 2nd-order resonance at 441nm has a minimum at the center of the cavity with two maxima on either side of it.

In our filter, tunability is introduced by inserting a thin layer of the GSST phase change material at the center of the cavity. Due to the field distribution, this GSST layer will have a large field overlap with the fundamental resonant field, and a minimal overlap with the 2nd order resonance. As a result, the fundamental resonance will be significantly affected by a phase change compared to the second order field. However, introducing an extra GSST layer, no matter how thin, will shift the original resonances slightly. But these can be easily accommodated by redesigning the dielectric and metal layer thicknesses using the same methodology outlined previously. Furthermore, to prevent additional intracavity resonances, it is important that the refractive index of the dielectric be similar to GSST. Also, it is important for the GSST layer to be very thin so that it can be fully contained within the minimum field intensity position of the 2nd order resonant field.

Figure 2(a) shows the redesigned contour plot for 850nm with a thin layer of GSST. As shown in Fig. 2(b), this has a fundamental resonance at 850nm and 2nd order resonance at 419nm. When the GSST layer switches from amorphous (represented as a-GSST) to crystalline (c-GSST) state, the fundamental resonance will be sufficiently disrupted by the large increase in refractive index and extinction coefficient. This makes the 850nm resonance to completely disappear. On the other hand, the resonance at 419nm will be preserved nearly at the same level as before. This can be verified from the field distribution plots in Figs. 2(c) and 2(d). As a result, we are able to realize a device that can switch between a high reflective state and a low reflective state at 850nm while preserving all the other features nearly the same.

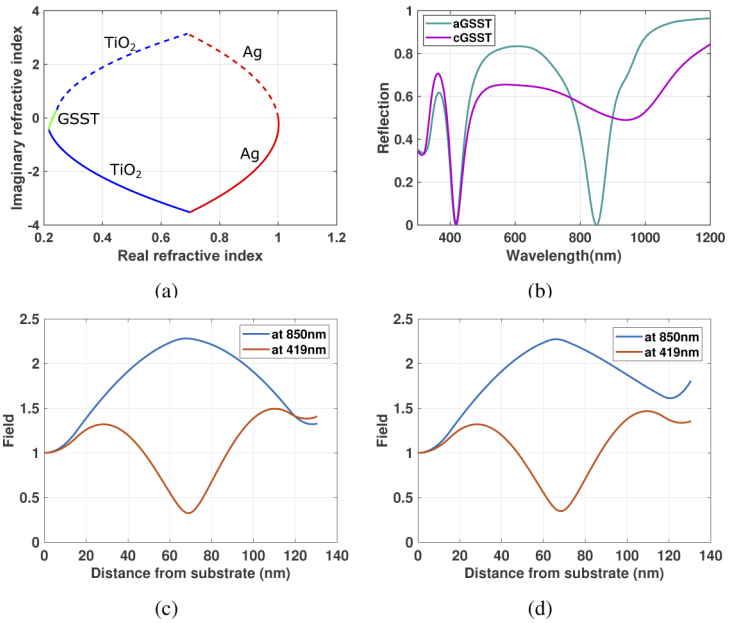

Fig. 2. (a) Solved contour of the structure after adding an a-GSST layer at the center of the cavity; (b) Reflection spectrum in the a-GSST and c-GSST states; Field plot for the cavity in the (c) a-GSST state, and (d) c-GSST state.

The dispersion data for GSST has been reported elsewhere in the literature [9]. Ellipsometric measurements of our GSST samples were found to be nearly identical to the values reported by others.

Optics EXPRESS

In order to produce a tunable filter for day and night time imaging applications, we used the structure in Fig. 2 as a baseline and further optimized it for a Si substrate with resonances at 850nm and 400nm. Since an oblique incidence is more convenient in a reflective configuration, we designed it for an incident angle of 45 degrees. The final structure is shown in Fig. 3.

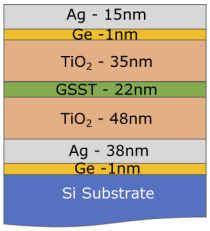

Fig. 3. Final layer structure of the filter with additional Ge layers to improve silver wetting designed for 45 degree incidence.

In this section, we have presented a systematic approach for designing a switchable reflective filter by starting from the simple MIM cavity, then introducing tunability by inserting a thin GSST layer, and finally redesigning the cavity for oblique incidence.

4. Device fabrication and testing

All the layers in the structure shown in Fig. 3 were fabricated using magnetron sputter deposition with Ar^+ ions. The GSST layer was deposited using a 3-inch GSST alloy target that was purchased from *Plasmaterials*. Using Energy Dispersive X-Ray Analysis (EDX), we verified the stoichiometry of the target and the resulting films to be $Ge_2Sb_2Se_4Te_1$. The deposition was carried out with an RF discharge power of 100W at 4mT pressure in an Ar^+ plasma. We measured the refractive indices of our GSST samples using ellipsometer and found to be nearly identical to the values reported in the literature [9]. TiO_2 was deposited using reactive sputtering between Ti and O_2. Thickness of each layer was measured after each deposition using a stylus profilometer for verification, and spectral measurements were taken using Filmertics reflection/transmission thin film analyzer. Overall performance of the final device was tested at both amorphous and crystalline states of GSST. In this work, we demonstrate the phase change effect by annealing the films on a hot plate. In practical implementations, this can be achieved with electrical joule heating or optical heating, which we did not attempt in this work.

Optical designs that use ultrathin silver layers are known to exhibit poor performance due to island or cluster formation. Several techniques have been proposed in the past to mitigate this issue. Typically, a very thin wetting layer (commonly using Cu, Ge, Cr, etc.) is introduced below the silver layer to improve the consistency of the silver film [15,16]. For this device, an addition of 1nm Ge layer was found to be the most effective with the least impact on the overall optical performance.

Two sets of samples were fabricated and one sample was heated on a hot plate at 300°C to induce the amorphous-to-crystalline phase transition. Then the reflection spectrum of these samples were measured and they were compared against the simulation results.

The crystalline-to-amorphous phase transition process requires a rapid melt-quench process that is significantly more complex than the amorphous-to-crystalline process. Nevertheless, both transitions are routinely employed in a number of applications, such as PCRAM and Bluray discs, as well as re-configurable meta-surfaces [10]. However, for this work, we have limited our demonstration to the the amorphous-to-crystal transition only.

During the actual fabrication of the devices, some thickness variations are unavoidable. Therefore, using a simple setup with a white light source, a base mirror and a spectrometer, the reflection spectrum of the fabricated filter was measured at different incident angles to choose

Optics EXPRESS

the best angle for our application. This is shown in Figs. 4(a) and 4(b). This angle was found to be 20 degrees. Therefore, all of the image demonstrations shown next were done at a 20 degree incident angle. Nevertheless, it should be pointed out that the angular sensitivity of this structure is quite small. This can be confirmed from the spectral plots shown in Figs. 4(a) and 4(b). This weak dependence is due to the small total film thickness used in our structure compared to the wavelengths of operation. This is consistent with the omnidirectional performance from ultrathin structures reported by others [17].

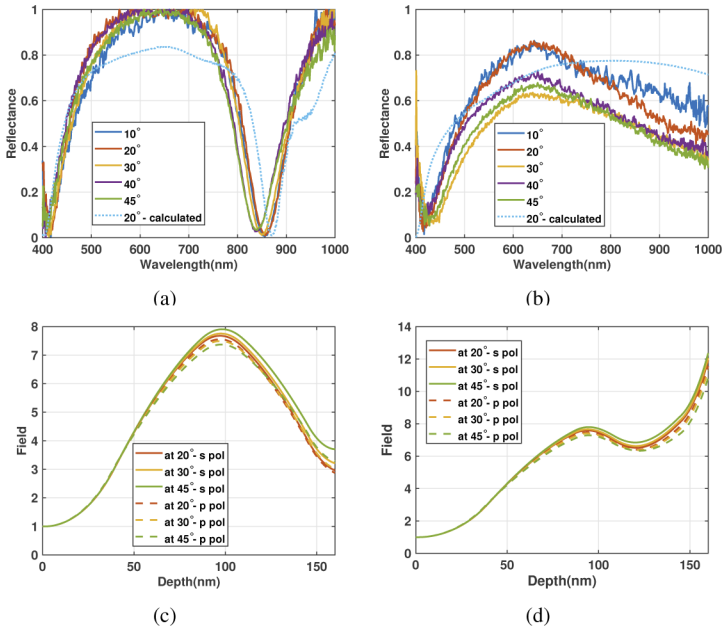

Fig. 4. Measured spectra of (a) a-GSST and (b) c-GSST filter samples at different incident angles, including the calculated values for 20 degree incidence of unpolarized light

5. Imaging demonstration

Our imaging configuration is shown in Fig. 5(a). The Midwest Optical Systems D850 filter is a dual-bandpass filter with the spectral transmission as shown in Fig. 6(a). This filter is designed to pass visible wavelengths in 405nm-645nm, as well as a LED or laser diode at 835nm-875nm, with peak transmission well above 90%. As evidenced in Fig. 6(b), the combination of D850 and a-GSST filters yield an overall effect that is similar to a conventional short-pass filter used in color cameras (passing visible wavelengths in 405nm-645nm while attenuating NIR completely). However, when the GSST is in the crystalline state, the combination of D850 and c-GSST passes 850nm LED or laser diode, as illustrated in Fig. 6(c). This configuration allows the silicon detector to be sensitive to an external NIR illumination source.

The camera used in our prototype system was FLIR Firefly S (FFY-U3-16S2C-C), a CMOS color image sensor. The NIR-cut filter supplied with the camera was removed. The lens was 12.5mm focal length Computar V1213. Two separate samples each at amorphous and crystalline sates of GSST were used for the image acquisition, to simulate the effect of a single GSST mirror that can perform amorphous-to-crystalline and crystalline-to-amorphous transformation. For a control imaging experiment, we also show the result of using Ag coated mirror (also fabricated in our laboratory) broadly reflecting light at wavelength range that silicon detectors are sensitive to.

Optics EXPRESS

Figure 7 shows a few images captured during the daytime and nighttime to assess the filtered imaging performance. Images were rendered with standard imaging pipeline, including black offset, demosaicking, color correction, white balance, and gamma correction. White balance in particular gives a *chance* at correcting unnatural colors in the daylight image (to the best of our ability, at least) in the presence of NIR light.

Owing to the high reflectivity of NIR wavelength on the leaves, combined with strong solar NIR illumination, the leaves render with strong violet hue in the control (Fig. 7(a)) and c-GSST

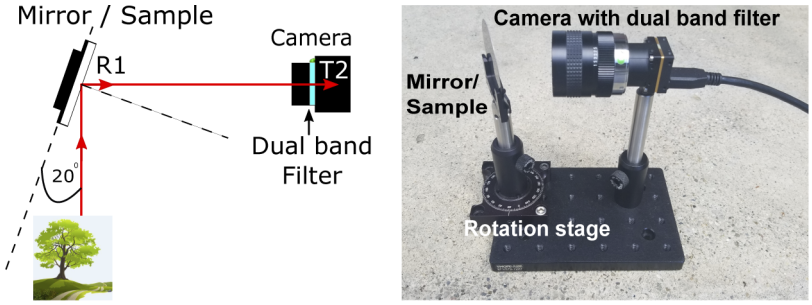

(a) (b)

Fig. 5. Prototype of the image demonstration setup. R1 is the reflection from the sample/mirror and T2 is the transmission through the dual band filter(D850).

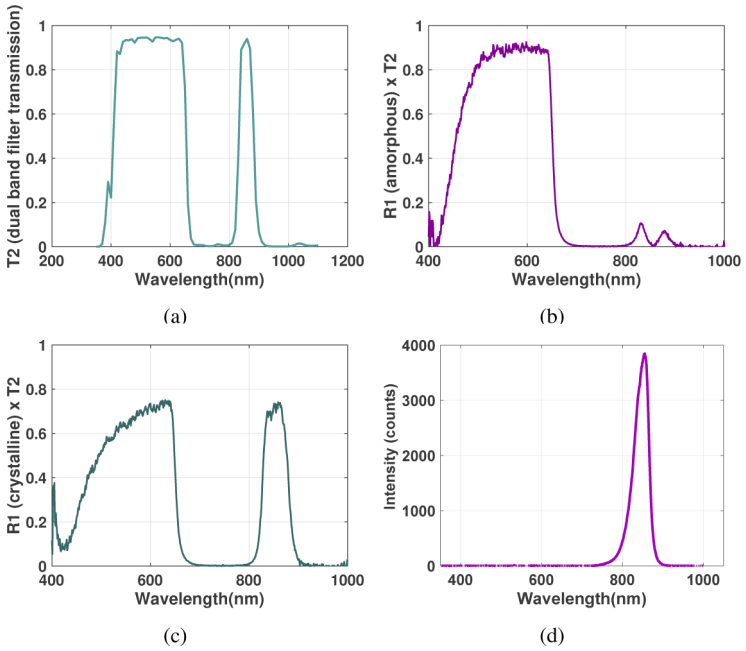

(a) (b) (c) (d)

Fig. 6. Measured spectra of filters used in the imaging configuration illustrated in Fig. 5. (a) Transmission spectra (T2) of Midwest Optical System D850 static filter. (b) Fraction of photons that reach the detector after reflecting from the GSST filter (amorphous state, or aGSST) and passing through D850 static filter (c) Fraction of photons that reach the detector after reflecting from the GSST (crystalline state, or cGSST) filter and passing through D850 static filter (d) Emission spectrum of the 850nm LED used in this experiment. All reflection and transmission values shown are in absolute units.

Optics EXPRESS

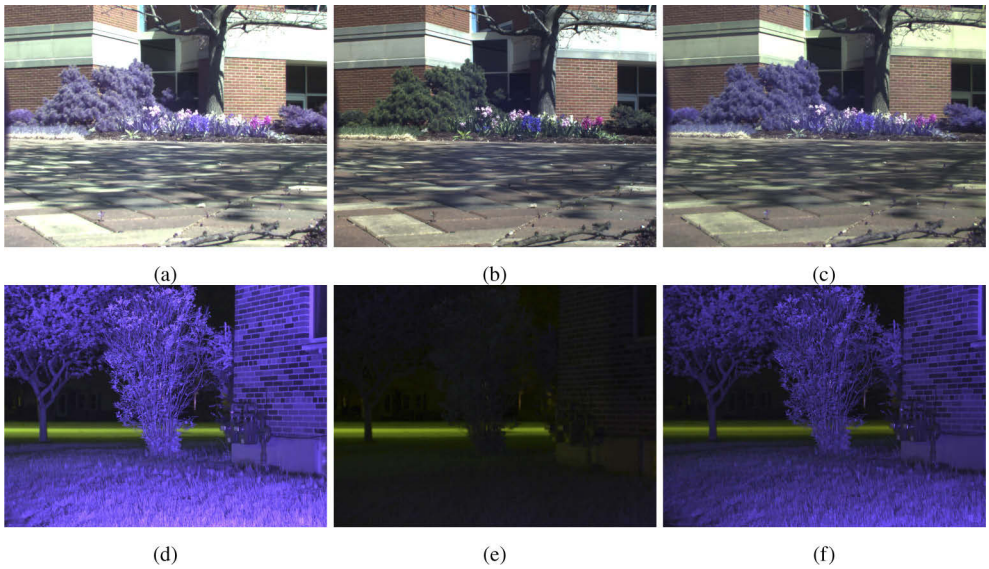

Fig. 7. Images captured by prototype system in Fig. 5. Daytime color images under solar illumination taken using (a) Ag control mirror, (b) a-GSST mirror, and (c) c-GSST mirror. Nighttime images with 850nm LED illumination taken using (d) Ag control mirror, (e) a-GSST mirror, and (f) c-GSST mirror. Due to the blocked NIR wavelengths, leaves in (b) appear green but image in (e) is dark.

(Fig. 7(c)) images. In contrast, the proposed a-GSST filter only passes visible light, allowing the color of leaves in Fig. 7(b) to be rendered green as we normally expect. Notice also that the purple flowers remain purple. On the other hand, the nighttime images are illuminated with a 850nm LED flood lamp (WAYLLSHINE E6). Under this scenario, the combination of D850 and a-GSST completely reject the NIR illumination source, yielding the dark image in Fig. 7(e). However, the camera configured with D850 and c-GSST successfully yield significantly brighter images (Fig. 7(f)), albeit the color of the objects are no longer represented (in night vision applications, these images would typically be rendered in grayscale). The images taken with D850 and the control Ag mirror in Fig. 7(d) are slightly brighter than the image Fig. 7(f). This is likely due to the c-GSST's small reflection loss in NIR wavelength range, as evidenced in Fig. 4(b).

6. Summary and conclusions

In this paper we have demonstrated a novel optical filter operating in the reflection mode with a tunable notch at 850nm. Its operation is based on the phase change material GSST. In its amorphous state, represented as a-GSST, the filter has zero reflection at 850nm. This blocks the near-infrared (NIR) light but keeps the visible wavelengths intact. In its crystalline state, representd as c-GSST, the filter has high reflectivity at 850nm which allows both the visible and NIR to be detected. We developed a prototype imaging system with daytime (color imaging) and nighttime (NIR illumination). Using a CMOS camera and visible + 850nm dual-bandpass filter, we demonstrated that color imaging is accurate during the daytime in the a-GSST state; and nighttime NIR imaging is possible in the c-GSST state with active 850nm illumination. We have only demonstrated the amorphous-to-crystalline phase transition in this study. In our future work, we plan to develop a melt-quench process to enable crystalline-to-amorphous phase transition. Additionally, while transmission mode filters are generally preferred in practical applications,

Optics EXPRESS

it is mathematically simpler to design layers for reflection, especially when layers with high absorption is involved. The resulting structures also have fewer layers than a transmission filter. For these reasons, we have focused on implementing a reflection mode filter in this paper.

Disclosures. The authors declare no conflicts of interest.

Data availability. Data underlying the results presented in this paper are not publicly available at this time but may be obtained from the authors upon reasonable request.

References

1. B. T. Kolomiets, "Vitreous semiconductors (i)," Phys. Status Solidi B **7**(2), 359–372 (1964).
2. N. Yamada, "Erasable phase-change optical materials," MRS Bull. **21**(9), 48–50 (1996).
3. C. Williams, N. Hong, M. Julian, S. Borg, and H. J. Kim, "Tunable mid-wave infrared fabry-perot bandpass filters using phase-change gesbte," Opt. Express **28**(7), 10583–10594 (2020).
4. M. N. Julian, C. Williams, S. Borg, S. Bartram, and H. J. Kim, "Reversible optical tuning of gesbte phase-change metasurface spectral filters for mid-wave infrared imaging," Optica **7**(7), 746–754 (2020).
5. N. Mou, X. Liu, T. Wei, H. Dong, Q. He, L. Zhou, Y. Zhang, L. Zhang, and S. Sun, "Large-scale, low-cost, broadband and tunable perfect optical absorber based on phase-change material," Nanoscale **12**(9), 5374–5379 (2020).
6. H. Zhang, L. Zhou, J. Xu, N. Wang, H. Hu, L. Lu, B. Rahman, and J. Chen, "Nonvolatile waveguide transmission tuning with electrically-driven ultra-small gst phase-change material," Sci. Bull. **64**(11), 782–789 (2019).
7. C. H. Chu, M. L. Tseng, J. Chen, P. C. Wu, Y.-H. Chen, H.-C. Wang, T.-Y. Chen, W. T. Hsieh, H. J. Wu, G. Sun, and D. P. Tsai, "Active dielectric metasurface based on phase-change medium," Laser Photonics Rev. **10**(6), 986–994 (2016).
8. Q. He, N. Youngblood, Z. Cheng, X. Miao, and H. Bhaskaran, "Dynamically tunable transmissive color filters using ultra-thin phase change materials," Opt. Express **28**(26), 39841–39849 (2020).
9. Y. Zhang, J. B. Chou, J. Li, H. Li, Q. Du, A. Yadav, S. Zhou, M. Y. Shalaginov, Z. Fang, H. Zhong, C. Roberts, P. Robinson, B. Bohlin, C. Ríos, H. Lin, M. Kang, T. Gu, J. Warner, V. Liberman, K. Richardson, and J. Hu, "Broadband transparent optical phase change materials for high-performance nonvolatile photonics," Nat. Commun. **10**(1), 4279 (2019).
10. Y. Zhang, C. Fowler, J. Liang, B. Azhar, M. Y. Shalaginov, S. Deckoff-Jones, S. An, J. B. Chou, C. M. Roberts, V. Liberman, M. Kang, C. Ríos, K. A. Richardson, C. Rivero-Baleine, T. Gu, H. Zhang, and J. Hu, "Electrically reconfigurable non-volatile metasurface using low-loss optical phase-change material," Nature Nanotechnology (2021).
11. Y. Qu, Q. Li, K. Du, L. Cai, J. Lu, and M. Qiu, "Dynamic thermal emission control based on ultrathin plasmonic metamaterials including phase-changing material gst," Laser Photonics Rev. **11**(5), 1700091 (2017).
12. S. G.-C. Carrillo, L. Trimby, Y.-Y. Au, V. K. Nagareddy, G. Rodriguez-Hernandez, P. Hosseini, C. Ríos, H. Bhaskaran, and C. D. Wright, "A nonvolatile phase-change metamaterial color display," Adv. Opt. Mater. **7**(18), 1801782 (2019).
13. A. Sarangan, "Design of metal-dielectric resonant-cavity thin-film structures using the effective reflectance index method," J. Opt. Soc. Am. B **35**(9), 2294–2301 (2018).
14. A. Sarangan, *Optical Thin Film Design* (1st ed.) (CRC Press, 2020).
15. W. Chen, M. D. Thoreson, S. Ishii, A. V. Kildishev, and V. M. Shalaev, "Ultra-thin ultra-smooth and low-loss silver films on a germanium wetting layer," Opt. Express **18**(5), 5124–5134 (2010).
16. C. Ni, P. Shah, and A. M. Sarangan, "Effects of different wetting layers on the growth of smooth ultra-thin silver thin films," Proc. SPIE **9170**, 91700L (2014).
17. R. Yang, C. Dai, C. Wan, G. Zheng, and Z. Li, "Planar ultrathin omni-directional perfect absorber utilizing amorphous silicon for photovoltaics," Opt. Mater. Express **10**(2), 532–539 (2020).